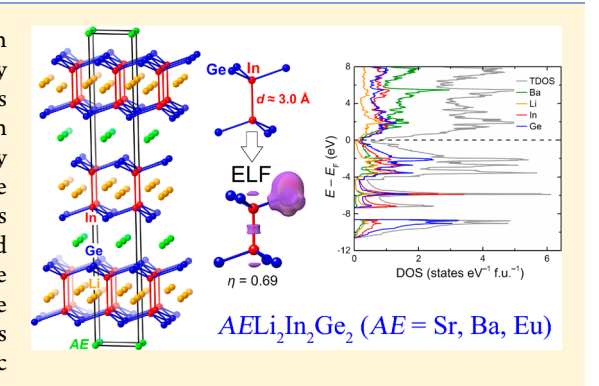
Inorganic Chemistry © Cite This: Inorg. Chem. XXXX, XXX, XXX–XXX

Layered Quaternary Germanides—Synthesis and Crystal and Electronic Structures of $AELi_2In_2Ge_2$ (AE = Sr, Ba, Eu)

Alexander Ovchinnikov^{†,‡} and Svilen Bobev*,[†]

Supporting Information

ABSTRACT: Three new quaternary germanides with the composition $AELi_2In_2Ge_2$ (AE = Sr, Ba, Eu) have been synthesized and structurally characterized. The layered crystal structure of these phases features homoatomic In—In bonding, but there are no direct Ge-Ge bonds. Such a crystallographic arrangement can be regarded as an ordered quaternary derivative of the $CaCu_4P_2$ structure (trigonal syngony, Pearson code hR7). Comprehensive analysis of the structural genealogy suggests relationships with the structures of other layered pnictides and chalcogenides, which are discussed. Partitioning of the available valence electrons and the assignment of the formal charges indicate that the composition of the new germanides is charge-balanced. First-principles calculations and electrical transport measurements indicate poor metallic behavior, resulting from significant hybridization of the electronic states.



INTRODUCTION

The continuous search for new ways of efficient energy storage has been a major topic in modern science for several decades. With the rapidly developing exploration of renewable energy sources, the need to accumulate energy for further transportation and consumption will undoubtedly grow in the near future. Currently, the most convenient way to store energy is in the form of electricity. This approach is realized in rechargeable batteries, with Li ion batteries dominating the market in this field.

Currently available electrode materials based on transition-metal oxides suffer from degradation upon electrochemical cycling, have low charging rates, and can be harmful for the environment. For these reasons, finding alternative materials is essential for the development of efficient energy storage systems. Several classes of compounds have been explored as possible candidates for these purposes. Among many others, bulk metal phosphides, nitrides, and chalcogenides as well as two-dimensional carbides and other carbon-based materials have been reported to display high performance in electrochemical tests, suggesting that non-oxide compounds can be promising replacements for the conventional oxide electrodes.

Recently, we embarked on studying Si and Ge clathrates for applications in electrochemical storage. The potential of such materials with an open framework was recently demonstrated for the metallic compositions Ba₈Al_ySi_{46-y} with the clathrate-I structure. This Si-based clathrate can be a suitable host for Li insertion and does not show considerable structural changes upon electrochemical cycling.⁵ By proper adjustment of the Al/Si ratio or introduction of dopants, charge-balanced

compositions can be produced. In such compositions, all atoms in the crystal structure adopt a closed-shell electron configuration, thereby optimizing the chemical bonding and driving the system to the semiconducting state. The described electronic situation constitutes the essence of the so-called Zintl concept, widely used to rationalize structures and compositions of intermetallic compounds. In contrast to the metallic Ba₈Al_ySi_{46-y}, the electron-precise Ba₈Al₁₆Si₃₀ performs relatively poorly in the lithiation process, unless an amorphous layer is present on the grain surfaces. Apparently, the reduction of the clathrate via Li insertion is unfavorable in this case, as it will disrupt the optimal electron count.

Different from Ba₈Al_ySi_{46-y}, upon lithiation, the Ge clathrate analogues have been found to undergo amorphization to an as yet unidentified Li-rich phase. The capacity of Ba₈Al_yGe_{46-y} decreases as the Al content is increased, which has been correlated with the decrease of framework vacancies in the material's crystal structure. Trying to resolve the potential phases that might form during the lithiation process, we set out to explore the Ba-Li-Al-Ge phase space. We focused our attention on the self-flux method, hypothesizing that in using it, less thermodynamically stable (i.e., kinetic) phases could be identified. However, the relatively high melting point and the very reducing nature of the molten Al metal presented experimental difficulties that hindered the synthesis steps. Therefore, in an effort to circumvent these challenges, we turned our attention to the Ba-Li-In-Ge system. Although it

Received: February 27, 2019



[†]Department of Chemistry and Biochemistry, University of Delaware, Newark, Delaware 19716, United States

[‡]Department of Materials and Environmental Chemistry, Stockholm University, Svante Arrhenius väg 16 C, 10691 Stockholm, Sweden

Table 1. Data Collection Details and Selected Crystallographic Data for AELi,In,Ge, (AE = Sr, Ba, Eu)^a

	$SrLi_2In_2Ge_2$	$BaLi_2In_2Ge_2$	$EuLi_2In_2Ge_2$
formula wt	476.32	526.04	540.66
a/Å	4.471(2)	4.520(2)	4.456(1)
c/Å	26.035(9)	26.836(9)	25.538(7)
$V/{ m \AA}^3$	450.7(3)	474.8(4)	439.2(3)
$ ho_{ m calc}/{ m g~cm}^{-3}$	5.27	5.52	6.13
$\mu_{ m MoK}\alpha/ m cm^{-1}$	261.1	225.4	283.0
R1 $(I > 2\sigma(I))^b$	0.018	0.023	0.017
wR2 $(I > 2\sigma(I))^b$	0.040	0.054	0.041
R1 (all data) ^b	0.018	0.025	0.017
wR2 (all data) b	0.040	0.055	0.042
$\Delta ho_{ m max,min}/{ m e}~{ m \AA}^{-3}$	0.95, -1.13	1.20, -1.98	1.08, -1.42

^aData for all compounds: space group $R\overline{3}m$, Z = 3, T = 200 K, Mo Kα with $\lambda = 0.71073$ Å. ${}^bR1 = \sum ||F_o| - |F_c|| / \sum |F_o|$; wR2 = $[\sum [w(F_o^2 - F_c^2)^2] / \sum [w(F_o^2)^2]]^{1/2}$, where $w = 1/[\sigma^2 F_o^2 + (AP)^2 + (BP)]$ and $P = (F_o^2 + 2F_c^2)/3$. A and B are the respective weight coefficients (see the CIF data).

has previously been studied, 9,10 after only a few tries, a new quaternary phase was successfully identified. An expansion of these studies to the Sr–Li–In–Ge and Eu–Li–In–Ge systems afforded two additional members of the series. These compounds, represented by the general formula AELi₂In₂Ge₂ (AE = Sr, Ba, Eu), are the main subject of this paper. They crystallize with a layered structure and formally can be considered as belonging to the family of Zintl phases.

In addition to the structure and chemical bonding of these layered germanides with homoatomic In—In bonding, presented and discussed as well are the preliminary studies on the versatility of this crystal structure. These results suggest that the $[In_2Ge_2]$ layers can adapt to small changes in the chemical composition and valence electron count. Specifically, the average structure appears to be retained upon the partial substitution of Li for In atoms (e.g., $[Li_{2+x}In_{2-x}Ge_2]$), making the $AELi_{2+x}In_{2-x}Ge_2$ solid solutions suitable candidates for further electrochemical studies. Such materials will likely be only of academic interest since they are expensive to make, and the prospects for their practical applications as battery electrodes are difficult to foresee.

EXPERIMENTAL DETAILS

Synthesis. Almost exclusively, procedures involving the starting materials and the final products were performed in an argon-filled glovebox or under vacuum. The reagents were purchased from Alfa, all with purity ≥99.9 wt %, and used as received.

Single crystals of $AELi_2In_2Ge_2$ (AE = Sr, Ba, Eu) were grown from excess In, intended as a flux. Mixtures of the elements in the ratio AE:Li:In:Ge = 1:12:20:2 were loaded in 2 cm³ alumina crucibles, which were subsequently placed in fused silica tubes and loosely covered with a piece of quartz wool, acting as a filter during the eventual centrifugation. The tubes were flame-sealed under vacuum, heated to 473 K at a rate of 10 K/h, and held at this temperature for 2 h to allow Li and In to melt. After that, the temperature was raised to 973 K at a ramp rate of 50 K/h. After annealing at this temperature for 10 h, cooling to 773 K was initiated at a rate of 5 K/h. At this point of the synthesis, the sealed tubes were taken out from the furnace and the molten metallic flux was separated from the crystals by centrifugation. A large excess of Li used in the reaction was necessary to compensate for the loss of Li due to evaporation and side reactions with the reactor walls. The tubes were break-opened inside the glovebox. The visually inhomogeneous solid product consisted of long intergrown gray crystals having a featherlike morphology and hexagonal black plates with metallic luster. The former type of crystals turned out to be the known binary compound LiIn, 11 as was confirmed by powder and single-crystal X-ray diffraction. Testing of the black plates on a single-crystal diffractometer revealed a

rhombohedral unit cell. The subsequent intensity data collection and the structure solution and refinement indicated a novel composition, AELi₂In₂Ge₂.

After the structure and the composition were deduced from singlecrystal diffraction work, efforts to produce the title compounds in bulk form by direct fusion of the respective elements were undertaken. For this purpose, stoichiometric mixtures of the elements were placed into Nb tubes that had been welded shut from one side. The tubes were filled with mixtures of the elements in the ratio AE:Li:In:Ge = 1:2:2:2 (weighing done in the glovebox), after which the tubes were sealed with an arc welder under partial pressure of high-purity argon gas. The welded Nb tubes were then enclosed in fused silica reactors, which were evacuated and flame-sealed (vacuum below discharge). After heating to 1023 K with 200 K/h and annealing for 48 h, the mixtures were cooled to 373 K at a rate of 5 K/h and removed from the furnace. The final products were multiphase mixtures, as revealed by powder X-ray diffraction. Careful analysis of the products by singlecrystal X-ray diffraction methods provided other important pieces of information, specifically that BaLi2+xIn2-xGe2 solid solutions with partial substitution of In by Li atoms exist.

Establishing the full homogeneity ranges in three quaternary systems is clearly an enormous task. Therefore, to keep with the scope of this exploratory study, detailed attempts were made to only alter the In to Li ratio in BaLi_{2+x}In_{2-x}Ge₂. This work was done in order to ascertain that a gradual structural transformation between two limiting compositions occurs. Such a line of thinking originates from the recognition of the fact that the structure of BaLi₂In₂Ge₂ (18 electrons/fu) and that of BaMg₂Li₂Ge₂ (16 electrons/fu)¹² bear a striking resemblance—notice that both structures are formally isotypic, but closer inspection reveals that certain aspects of their crystal chemistry are different (vide infra), which is certainly due to the different valence electron counts. Therefore, polycrystalline samples with the nominal compositions BaLi_{2.67}In_{1.33}Ge₂ and BaLi₃InGe₂ were prepared by following the protocols mentioned earlier. The sample "BaLi_{2.67}In_{1.33}Ge₂" yielded the desired Ba- $\text{Li}_{2+x}\text{In}_{2-x}\text{Ge}_2$ phase as the major product $(x \approx 0.54)$, whereas the main phases observed in the PXRD pattern of the Li-richer "BaLi₃InGe₂" specimen were BaLi_{1-x}In_xGe₂, ¹¹ BaGe₂, ¹³ and Ba₈Ge_{46-x}In_x. ¹⁴ BaLi_{2+x}In_{2-x}Ge₂ ($x \approx 0.66$) was identified as a minor phase, being distinguished from the three other compounds by the platelike morphology of the grown crystals that could be easily identified under an optical microscope.

During the numerous tries to optimize reactions in Nb tubes, yet another phase, $BaLi_{1.02(2)}In_{0.98}Ge_2$, was identified as a side product. A similar compound, $BaLi_xIn_{2-x}Ge_2$ ($x\approx 1$), has previously been described to crystallize in the $ThCr_2Si_2$ structure type. 10 From the experiments described above, a partially ordered solid solution crystallizing in a superstructure of the common body-centered-tetragonal $ThCr_2Si_2$ structure was afforded.

Attempts to expand the AELi₂In₂Ge₂ series to include Ca from the alkaline-earth metals and Yb from the lanthanides, which nominally

Table 2. Data Collection Details and Selected Crystallographic Data for $BaLi_{2+x}In_{2-x}Ge_2$ (x = 0.54(1), 0.66(1)) and $BaLi_{1.02(2)}In_{0.98}Ge_2^a$

	$BaLi_{2.54(1)}In_{1.46}Ge_2$	$BaLi_{2.66(1)}In_{1.34}Ge_2$	$BaLi_{1.02(2)}In_{0.98}Ge_{2} \\$
formula wt	468.14	454.84	401.85
space group	$R\overline{3}m$	$R\overline{3}m$	P4 ₂ /mcm
a/Å	4.5747(6)	4.5742(4)	6.629(1)
c/Å	26.381(4)	26.263(2)	11.163(2)
$V/{ m \AA}^3$	478.1(1)	475.89(9)	490.5(2)
Z	3	3	4
$ ho_{ m calc}/{ m g~cm}^{-3}$	4.88	4.76	5.44
$\mu_{ m MoK}\alpha/{ m cm}^{-1}$	204.9	201.5	244.0
R1 $(I > 2\sigma(I))^b$	0.015	0.014	0.025
wR2 $(I > 2\sigma(I))^b$	0.038	0.030	0.085
R1 (all data) ^b	0.015	0.016	0.033
wR2 (all data) ^b	0.038	0.030	0.091
$\Delta ho_{ m max,min}/{ m e}~{ m \AA}^{-3}$	0.75, -1.10	1.12, -0.61	0.94, -1.24

"Data for all compounds: T = 200 K, Mo K_{α} with $\lambda = 0.71073 \text{ Å}$. ${}^{b}R1 = \sum ||F_{0}| - |F_{c}|| / \sum |F_{0}|$; $wR_{2} = [\sum [w(F_{0}^{2} - F_{c}^{2})^{2}] / \sum [w(F_{0}^{2})^{2}]]^{1/2}$, where $w = 1/[\sigma^{2}F_{0}^{2} + (AP)^{2} + (BP)]$, and $P = (F_{0}^{2} + 2F_{c}^{2})/3$; A, B are the respective weight coefficients (see the CIF data).

behaves as a divalent ion in germanides, were unsuccessful. Both the flux and the traditional high-temperature methods were tried. In addition to the simple binary germanides, among the products of these reactions, the quaternary phases $\text{Ca}_2\text{LiInGe}_2$ and $\text{Yb}_2\text{LiInGe}_2$ were also identified—both of their structures are known 15,1 δ and do not appear to form with Ba.

Powder X-ray Diffraction (PXRD). PXRD patterns were taken on a Rigaku Miniflex diffractometer (Cu K α radiation, $\lambda = 1.5418$ Å) operating inside a nitrogen-filled glovebox. Data were collected in the θ - θ scan mode with a step size of 0.05° and 2 s/step counting time. The PXRD patterns were only used for phase identification. Data gathered for samples as prepared, those treated under an inert atmosphere and those exposed to ambient air for 24 h suggest that the title compounds are air-sensitive and decompose if not handled properly.

Single-Crystal X-ray Diffraction (SCXRD). Single crystals were handled under dry Paratone-N oil. Suitable crystals were cut to the desired dimensions and mounted on low-background plastic loops for measurements. Data collection was performed in a stream of cold nitrogen at T = 200 K on a Bruker SMART APEX CCD diffractometer equipped with monochromated Mo K α radiation (λ = 0.71073 Å). Data integration and correction for absorption were done with the SAINT¹⁷ and SADABS¹⁸ software packages, respectively. Crystal structures were solved by dual-space methods as implemented in SHELXT¹⁹ and refined by full-matrix least-squares methods on F² with SHELXL.²⁰ All atoms, including Li, were refined anisotropically. For the structures with mixed occupied Li/In positions, the site occupancy factors (SOF) were first refined freely to establish the range of the deviations and then corefined with SOFs summed to 100%, with no additional constraints used. Before the final refinements, atomic coordinates and labels were standardized using the STRUCTURE TIDY program.²¹ Details of the data collection and other relevant crystallographic parameters are given in Tables 1-4. CIFs have also been deposited with reference numbers in the sequence from 1899716-1899721.

Atomic coordinates and selected interatomic distances for $BaLi_{1.02(2)}In_{0.98}Ge_2$ are summarized in Tables S1 and S2 in the Supporting Information, along with a schematic representation of this crystal structure (Figure S1).

Scanning Electron Microscopy. Selected single crystals from different batches were examined on a JEOL JSM-6335F scanning electron microscope, equipped with an energy-dispersive X-ray (EDX) spectrometer. The semiquantitative EDX analysis only confirmed the expected ratios of the heavy elements. The amount of Li (Z = 3) could not be verified by this method.

First-Principles Calculations. Electronic structures were calculated for BaLi₂In₂Ge₂ and SrLi₂In₂Ge₂ within the density functional theory framework (DFT) employing the TB-LMTO-ASA code.²² For

Table 3. Atomic Coordinates and Equivalent Displacement Parameters ($Å^2$) for $AELi_2In_2Ge_2$ (AE = Sr, Ba, Eu)

atom	site	x	y	z	$U_{ m eq}^{a}$		
$SrLi_2In_2Ge_2$							
Sr	3a	0	0	0	0.0106(3)		
Li	6c	0	0	0.1500(5)	0.027(4)		
In	6c	0	0	0.44159(2)	0.0127(3)		
Ge	6c	0	0	0.25849(3)	0.0098(3)		
			BaLi ₂ In	$_2$ Ge $_2$			
Ba	3a	0	0	0	0.0115(3)		
Li	6c	0	0	0.156(2)	0.09(2)		
In	6c	0	0	0.44355(3)	0.0137(3)		
Ge	6c	0	0	0.25520(5)	0.0110(3)		
			EuLi ₂ In	$_2$ Ge $_2$			
Eu	3 <i>a</i>	0	0	0	0.0087(2)		
Li	6c	0	0	0.153(1)	0.058(7)		
In	6c	0	0	0.44042(2)	0.0121(2)		
Ge	6c	0	0	0.26076(4)	0.0094(3)		

 $^{a}U_{\mathrm{eq}}$ is defined as one-third of the trace of the orthogonalized U_{ij}

Table 4. Atomic Coordinates and Equivalent Displacement Parameters (Å²) for $BaLi_{2+x}In_{2-x}Ge_2$ ($x \approx 0.54, 0.66$)

atom	site	x	у	z	$U_{ m eq}^{a}$
		Ba	Li _{2.54(1)} In	_{1.46} Ge ₂	
Ba	3 <i>a</i>	0	0	0	0.0106(2)
Li	6c	0	0	0.1447(4)	0.025(2)
In/Li ^b	6c	0	0	0.44032(2)	0.0127(2)
Ge	6c	0	0	0.25017(2)	0.0112(2)
		Ba	Li _{2.66(1)} In	$_{1.34}$ Ge ₂	
Ba	3 <i>a</i>	0	0	0	0.0115(2)
Li	6c	0	0	0.1438(5)	0.024(3)
In/Li^c	6c	0	0	0.43866(3)	0.0139(3)
Ge	6c	0	0	0.24882(3)	0.0117(2)

 $^aU_{\rm eq}$ is defined as one-third of the trace of the orthogonalized U_{ij} tensor. $^b{\rm In/Li}=0.731(2){\rm In}+0.269{\rm Li.}$ $^c{\rm In/Li}=0.670(3){\rm In}+0.330{\rm Li.}$

comparison, the electronic density of states (DOS) was evaluated also for the structurally related $BaMg_2Li_2Ge_2$. The von Barth–Hedin version of the local density approximation functional (LDA) was used. To satisfy the atomic sphere approximation (ASA), the introduction of empty spheres was executed with the automatic

procedure implemented in the LMTO code. The Brillouin zone was sampled by a $24 \times 24 \times 24$ *k*-point grid after checking for convergence.

Chemical bonding was examined using crystal orbital Hamilton population curves (COHP) and electron localization function (ELF), which were calculated with the dedicated modules of the LMTO program. Bader charges were calculated with the program Critic2. For the integration, the primitive cell was sampled by a 350 \times 350 point grid.

Electrical Transport Measurements. The temperature dependence of electrical resistivity was measured only for a small, bar-shaped single crystal from the SrLi₂In₂Ge₂ sample. Crystals of BaLi₂In₂Ge₂ and EuLi₂In₂Ge₂ were not suitable—they were either too air-sensitive (Ba) or too small (Eu); hence, no electrical contacts could be placed on them. The measurements were carried out in the temperature range 10–300 K, using a four-probe setup on a Quantum Design Physical Property Measurement System (PPMS). The surface of the crystal was gently cleaned using fine-grit sandpaper and rinsing with dry acetone. Platinum-metal wires were attached using a conductive silver paint. The measurements were performed upon cooling and heating to ensure reproducibility.

RESULTS AND DISCUSSION

The $AELi_2In_2Ge_2$ compounds (AE = Sr, Ba, Eu) crystallize in space group $R\overline{3}m$ (No. 166), and the structure is schematically shown in Figure 1(a). There are four independent positions in

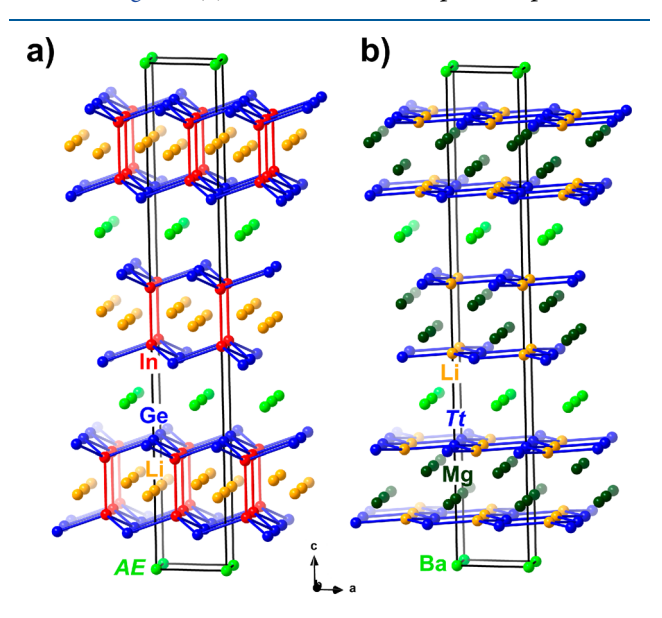


Figure 1. Crystal structures of $BaLi_2In_2Ge_2$ (a) and of $BaMg_2Li_2Si_2$ and $BaMg_2Li_2Ge_2$ (b). The symmetry-unique atomic positions are labeled.

the asymmetric unit—one for each atom of the respective elements (Table 3)—and the corresponding Pearson code is hR7. The crystal structure can be regarded as an ordered quaternary variant of the $CaCu_4P_2$ structure (Figure 2a,b). The anionic substructure consists of two-dimensional slabs built up of ethane-like In_2Ge_6 units in a staggered conformation linked via Ge atoms. The lithium atoms reside within the slabs, whereas the larger AE atoms are located in the space between adjacent slabs. The arrangement of the Ge atoms resembles a distorted hexagonal close packing. In this description, the Li atoms occupy half of the tetrahedral voids and the AE atoms fill half of the octahedral cavities in an alternating layer-by-layer manner along the c direction (in the hexagonal setting). Each In atom has a pseudotetrahedral

coordination by three near-neighbor Ge atoms and an In atom. Thus, due to the presence of an In–In bond, a charge of +2 should be assigned to the In atoms, leading to the electron-precise notation $(AE^{2+})(\mathrm{Li}^+)_2(\mathrm{In}^{2+})_2(\mathrm{Ge}^{4-})_2$. Alternatively, the valence electrons can be partitioned as follows: $(AE^{2+})(\mathrm{Li}^+)_2[(4b\mathrm{-In}^{1-})_2(3b\mathrm{-Ge}^{1-})_2]$, where polyanionic $[\mathrm{In}_2\mathrm{Ge}_2]^{4-}$ layers are considered, in which the atoms of In (4-bonded) and Ge (3-bonded) are assigned a formal charge of -1 each. The derived formal charge distribution suggests that the $AE\mathrm{Li}_2\mathrm{In}_2\mathrm{Ge}_2$ ($AE=\mathrm{Sr}$, Ba, Eu) compositions belong to the broad class of Zintl phases.

A similar crystal structure is adopted by the quaternary compositions BaMg₂Li₂ Tt_2 (Tt = Si, Ge), ¹² as shown in Figure 1b. Formally, the two structures are isopointal, but from the chosen projections in Figure 1, one can readily notice that the Mg and Li atomic positions in BaMg₂Li₂ Tt_2 are interchanged relative to the Li and In positions in AELi2In2Ge2. In other words, in the former structure, the Li atoms are trigonally coordinated by the tetrel element, while in AELi₂In₂Ge₂, similar coordination is observed for the In atoms. It is worth noting that the Li atoms in $BaMg_2Li_2Tt_2$ reside in trigonalplanar $LiTt_3$ units forming almost flat layers with no direct Li-Li interactions (the separation between adjacent layers is too great, more than 3.6 Å in the case of BaMg₂Li₂Ge₂).¹² As discussed above, this is not the case in AELi₂In₂Ge₂, where the In atoms are tetrahedrally coordinated (three closer Ge neighbors and a bit more distant In-vide supra) and double layers of corrugated InGe sheets are formed. The apparent requirement for a charge-balanced composition calls for divalent cations in the intralayer space; hence, Mg is present in place of Li, resulting in the electron-precise formula $(Ba^{2+})(Mg^{2+})_2(Li^+)_2(Tt^{4-})_2.$

By imaginary removal of the Li atoms from the $AE\text{Li}_2\text{In}_2\text{Ge}_2$ structure, the composition $AE\text{In}_2\text{Ge}_2$ can be derived. To sustain the charge balance without perturbing the homoatomic bonding in the slabs, Ge ought to be replaced by a group 15 element which will have one more valence electron. Indeed, the envisioned "1-2-2" structure is adopted by the ternary Zintl phase $\text{CaGa}_2\text{As}_2 \equiv (\text{Ca}^{2+})(\text{Ga}^{2+})_2(\text{As}^{3-})_2,^{26}$ where Ca and Ga isovalently replace heavier AE and In, respectively, and As aliovalently replaces Ge (Figure 2c). Note that, in the electron-partitioning scheme above, Ga in CaGa_2As_2 is assigned a charge of +2 due to the presence of Ga—Ga bonds, just like the In atoms in $AE\text{Li}_2\text{In}_2\text{Ge}_2$. In accordance with the charge-balanced formula for CaGa_2As_2 , first-principles calculations reveal that the Fermi level in this compound is located inside a deep pseudogap.

In the example above, the crystal structure of $CaGa_2As_2$ was derived from that of $AELi_2In_2Ge_2$ by imaginary cation extraction and element substitution, while the structure and stacking of the two-dimensional anionic slabs are preserved. Following this line of thinking, it is possible to imagine a structure where the interlayer cations are also removed, leaving a van der Waals gap between the slabs. To preserve the electron count, such a transformation would require a chalcogen atom (group 16 element) in place of the As atom, if one considers the $CaGa_2As_2$ structure as an intermediate step in this Gedanken experiment. In fact, the hypothetical structure constructed this way is adopted by the metastable gallium sulfide $GaS(3R) \equiv Ga_2S_2$, which can be similarly formulated as an electron-precise compound, $(Ga^{2+})_2(S^{2-})_2$ (Figure 2d).²⁷

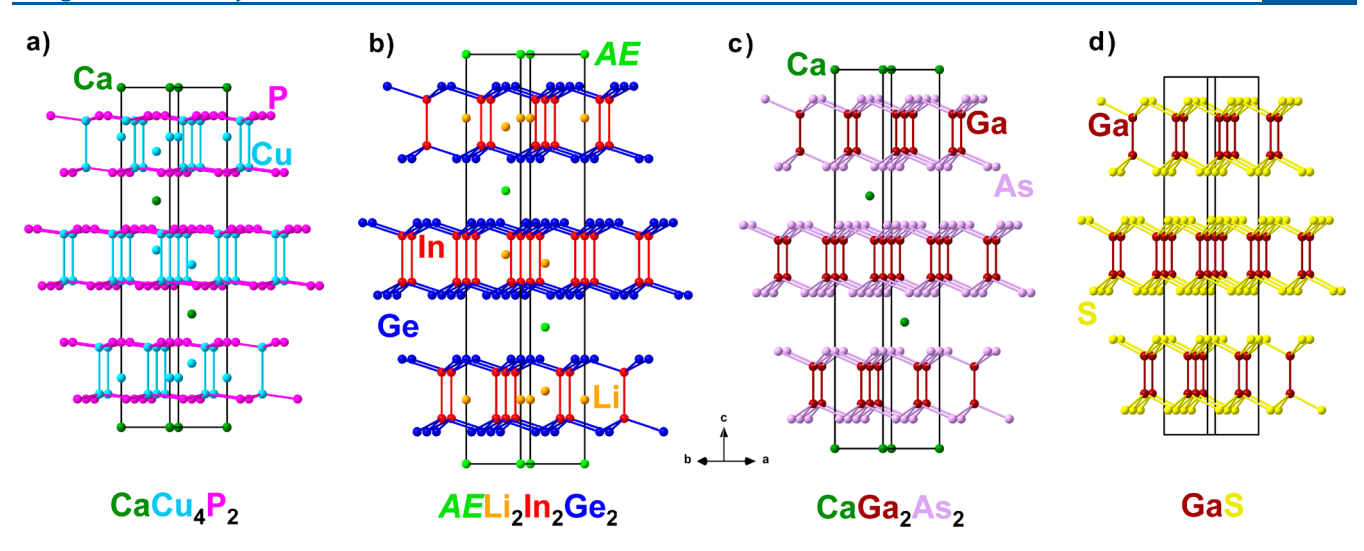


Figure 2. Structural relationships among (a) CaCu₄P₂, (b) AELi₂In₂Ge₂ (AE = Sr, Ba, Eu), (c) CaGa₂As₂, and (d) GaS.

Table 5. Selected Interatomic Distances (Å) for $AELi_2In_2Ge_2$ (AE = Sr, Ba, Eu) and $BaLi_{2+x}In_{2-x}Ge_2$ ($x \approx 0.54$, 0.66)

atoms	AE					
	Sr	Ba	Eu	Ba $(x = 0.54(1))$	Ba $(x = 0.66(1))$	
AE -Ge \times 6	3.2343(9)	3.348(1)	3.1708(9)	3.4336(5)	3.4497(5)	
AE -In \times 6	3.8220(8)	3.944(1)	3.7547(9)	3.8654(5)	3.8243(5)	
$Li-In \times 3$	2.801(6)	2.88(3)	2.82(1)	2.822(4)	2.828(5)	
$Li-In \times 3$	3.237(9)	3.18(3)	3.19(2)	3.409(7)	3.445(8)	
Li-Ge	2.82(1)	2.67(6)	2.76(3)	2.78(1)	2.76(1)	
Li−Ge × 3	3.239(9)	3.34(3)	3.29(2)	3.100(6)	3.066(6)	
$In-Ge \times 3$	2.7239(9)	2.748(1)	2.7195(8)	2.7149(4)	2.6969(3)	
In-In	3.041(2)	3.030(2)	3.043(1)	3.149(1)	3.222(1)	

Early attempts to synthesize the AELi₂In₂Ge₂ compositions by conventional high-temperature annealing produced samples with varying unit cell parameters for a given AE metal used, suggesting that a possible homogeneity range exists. Since Li is known to substitute for certain p elements, e.g., Ga, ²⁸ In, ^{9,29} and Sn, 30 in the crystal structures of intermetallic compounds, directed synthesis of Li-substituted samples with the nominal general composition BaLi_{2+x}In_{2-x}Ge₂ was carried out in sealed tubes. Careful crystal structure analysis confirmed partial replacement of In by Li atoms, with no other sites in the structure displaying mixed occupation (Table 4). As the Li occupancy of the In site increases, the formal positive charge of this position is expected to be reduced, thereby driving the system out of the charge-balanced state to the electron-poorer region. To counteract this effect, the distance between the bound In atoms elongates, weakening the In-In interaction and supplying electrons necessary to retain the charge balance. Upon going from BaLi₂In₂Ge₂, which is devoid of disorder, to the solid solution BaLi_{2+x}In_{2-x}Ge₂ ($x \approx 0.66$), the In-In interatomic separation changes from 3.03 to 3.22 Å, respectively. From the above, it might be reasoned that the In-In contact can no longer be viewed as a two-center, twoelectron bond. These metrics ought to be compared with caution, of course, since from the structure refinements it is apparent that the In position ca. 30% of the time is occupied by a Li atom—this renders the description of In2 dimers in BaLi_{2+x}In_{2-x}Ge₂ somewhat ambiguous, since the Li substitution leads to loss of In-In contacts and the manifestation of In-Li contacts. Even the less probable Li-Li pairs will be statistically possible. Thus, there are two basic ways such an

effect on the distances can be rationalized. (1) By exaggeration of the ionicity of the bonding in this compound, its composition can be represented as (Ba2+)- $(Li^{+})_{2.66}(In^{2.49+})_{1.34}(Ge^{4-})_{2}$, where the fractional formal charge of In reflects this peculiar bonding situation. In the limiting case, when homoatomic In-In bonding is absent, the In atoms would be assigned as +3, as expected from the charge-balanced formula $(Ba^{2+})(Li^+)_3(In^{3+})Ge_2$. In other words, in order to understand the structural change, which accompanies the partial replacement of In atoms by Li atoms on the In site of the structure, one has to view it as the result of a formal oxidation process (BaLi₂In₂Ge₂ has a total of 18 electrons/fu, while BaLi_{2+x}In_{2-x}Ge₂ ($x \approx 0.66$) has ca. 16.7 electrons). (2) Alternatively, when the covalency of the bonding is exaggerated31 and an In:Li ratio of 2:1 is considered, the following formula breakdown can be proposed: (AE^{2+}) - $(Li^{+})_{2.66}[(4b\text{-}In^{1-})_{0.67}(3b\text{-}In^{0})_{0.67}(3b\text{-}Ge^{1-})_{1.33}(0b\text{-}Ge^{4-})_{0.67}].$ In the case of BaLi₃InGe₂, i.e., the structure where exactly half of the In atoms are replaced by Li atoms and homoatomic In-In bonding can be completely avoided, the formula could be expressed as $(AE^{2+})(\hat{L}i^{+})_{3}[(3b-\text{In}^{0})(3b-\text{Ge}^{1-})(0b-\text{Ge}^{4-})].$ From this point of view, the covalent $[In_2Ge_2]^{4-}$ layers in BaLi₂In₂Ge₂ will become [InGe₂]⁵⁻ in BaLi₃InGe₂: i.e., a formal chemical reduction should be considered. The latter process must be accompanied by lone pair formation or some other localized electronic feature at the Ge and In sites, which neighbor the "extra" Li.

Following the preceding discussion, one might hypothesize that two compounds with compositions that satisfy/validate the presented arguments would be likely to exist: (1)

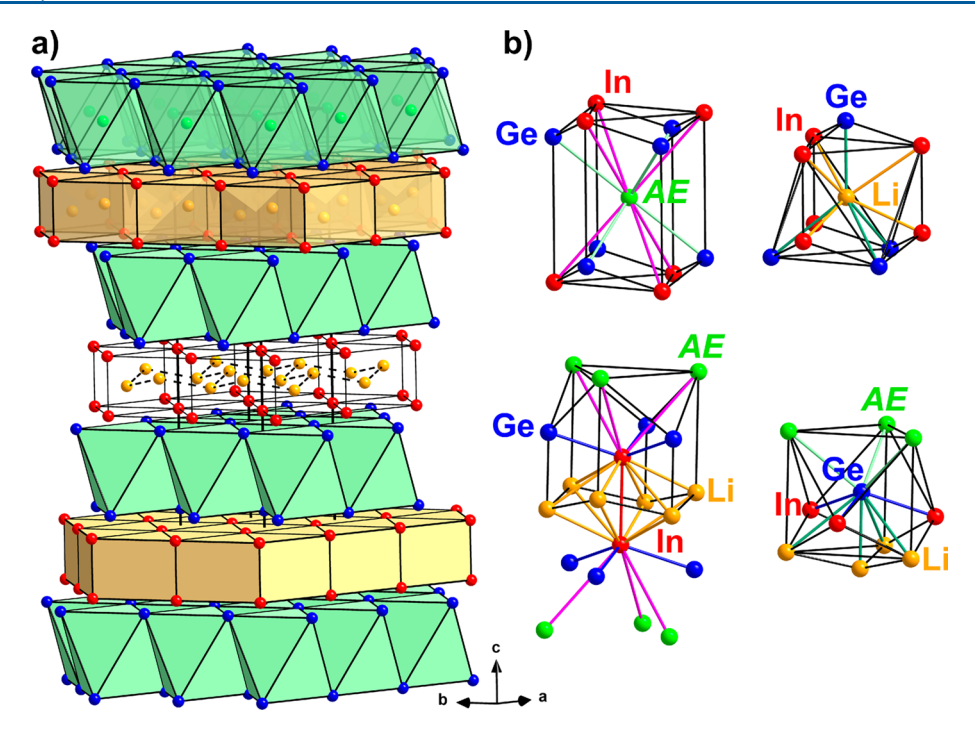


Figure 3. (a) Crystal structure of $AELi_2In_2Ge_2$ (AE = Sr, Ba, Eu) viewed as a stacking of $[AEGe_2]$ (green) and $[Li_2In_2]$ (orange) slabs. (b) Coordination environment of the atomic sites in $AELi_2In_2Ge_2$.

BaLi₃InGe₂, which was discussed in the context of a limiting case for the solid solution $BaLi_{2+x}In_{2-x}Ge_2$ (x = 1), i.e., the structure where exactly half of the In atoms are replaced by Li, and (2) BaIn₂Ge₂, where all the Li atoms are removed from the parent BaLi₂In₂Ge₂ structure. Up until now, neither these compositions nor their imaginary solid solution BaLi_{3x}In_{2-x}Ge₂ has been experimentally observed. From our inability to prepare these compounds and from the apparent destabilization of the overall electronic structure when the In-In interactions are disrupted, it can be surmised that the weakened In–In bonding in BaLi_{2+x}In_{2-x}Ge₂ ($x \approx 0.66$) represents a two-center, one-electron interaction: i.e., a single electron is occupying the bonding state. As such, this composition can be suggested to be the boundary of existence of this structure—beyond it, bonding patterns similar to those already discussed could be realized but with different elements, as shown by the example of BaMg₂Li₂Ge₂. If

Another view of the crystal structure of $AELi_2In_2Ge_2$ (AE = Sr, Ba, Eu) suggests that it can be considered a stacking sequence of alternating isolated rock-salt-type [$AEGe_2$] and anti-AlB₂-type [Li_2In_2] slabs. In contrast to the planar B sheets in AlB₂, the Li atoms here form a rippled hexagonal net, similar to the Ge network in the EuGe₂ structure (Figure 3a). 32

The described representation of the structure provides visualization of the local coordination environment for the cation sites. The AE-Ge contacts for all studied compounds fall in the typical range of bonding distances found in other AE germanides. $^{9,10,12,13,32-35}$ The octahedral coordination of the AE atoms in AELi₂In₂Ge₂ can be extended by including the six In atoms from the adjacent [Li₂In₂] slabs (Figure 3b, top left). The corresponding AE-In distances are somewhat longer than the typical bonding contacts (Table 5). However, several AE indides with elongated AE-In bonds have been reported. $^{36-38}$ Our first-principles calculations indicate that the AE-In interactions do show bonding character, although they are comparably weak (vide infra).

The Li atoms reside in a distorted-trigonal-prismatic coordination of the In atoms. In addition, four Ge atoms are located in the vertices of a distorted tetrahedron around every Li atom (Figure 3b, top right). Three out of six Li-In distances are virtually unaffected by the AE metal or Li/In mixing in the substituted series and measure about 2.8 Å, in good agreement with the sum of the single-bonded Pauling radii ($r_{\rm Li}$ = 1.23 Å, $r_{\rm In}$ = 1.50 Å³⁹). The remaining three Li–In contacts preserve approximately the same lengths of about 3.2 Å for the unsubstituted AELi₂In₂Ge₂ phases but stretch up to more than 3.4 Å in the solid solution $BaLi_{2+x}In_{2-x}Ge_2$ ($x \approx$ 0.54, 0.66), concomitant with the elongation of the In-In bond: i.e., the height of the LiIn₆ trigonal prism. An opposite trend is observed for the Li-Ge contacts. One of the four Li-Ge distances stays almost the same for all studied compositions, with $d_{\text{Li-Ge}} \approx 2.7 - 2.8$ Å, which is somewhat longer than the sum of the atomic radii ($r_{Li} = 1.23 \text{ Å}, r_{Ge} = 1.22$ Å³⁹) but falls in the usual range of bonding Li–Ge contacts in other lithium germanides. ^{19,10,33,34,40,41} The other three Li–Ge distances range from 3.2 to 3.3 Å in the AELi₂In₂Ge₂ compositions and decrease considerably upon introducing Li on the In site, dropping to about 3.1 Å for the solid solution BaLi_{2+x}In_{2-x}Ge₂ ($x \approx 0.54$, 0.66). These changes result in a more regular shape of the LiGe₄ tetrahedron and stronger Li-Ge bonding, while at the same time, the distortion of the LiIn₆ trigonal prism leads to weakening of some of the Li-In interactions. Apparently, such variations of the interatomic distances retain the electrostatic potential of the formally cationic Li⁺ and optimize the bonding.

Electronic Structure and Chemical Bonding. The electronic density of states (DOS) for $BaLi_2In_2Ge_2$ is shown in Figure 4a. Although the formal electron counting yields a charge-balanced composition, which would suggest a semiconducting ground state, $BaLi_2In_2Ge_2$ displays a pseudogap at the Fermi level (E_F), and therefore metallic behavior is expected for this phase. This apparent "contradiction" is a

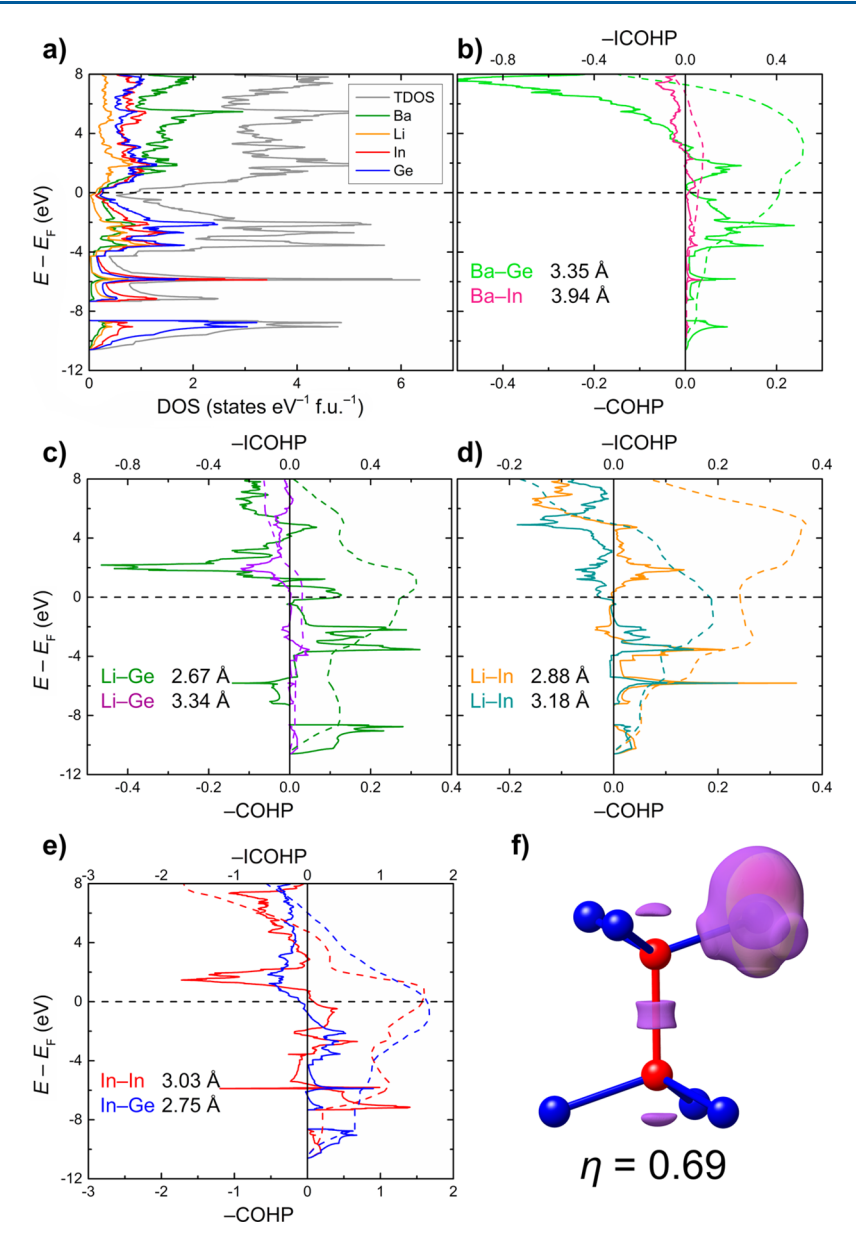


Figure 4. (a) Electronic density of states (DOS) for $BaLi_2In_2Ge_2$. (b–e) Crystal orbital Hamilton population curves (COHP) for selected interactions. (f) Electron localization function (ELF) in the vicinity of an In_2Ge_6 unit in $BaLi_2In_2Ge_2$ evaluated at the η = 0.69 isosurface level. For clarity, the ELF distribution around only one of the Ge atoms is shown.

known shortcoming of the Zintl approach, which simply overestimates the extent to which an electron transfer occurs between the cations and anions. If significant orbital hybridization between the formally cationic and anionic units develops, smearing of the electronic states may close the band gap that would otherwise be observed for highly polar bonding. In fact, metallic Zintl phases are not unusual per se and have been described in various chemical systems.³¹ In many cases, isostructural compounds display a crossover from semiconducting to metallic behavior upon replacement of the nonmetal or metalloid element constituting the Zintl anion with congeners from later periods, as this change is accompanied by a decrease in the bonding ionicity.⁴ Zintl tetrelides, i.e., compounds with group 14 anions, metallic properties are also frequently observed despite the formal charge balance. 32,43,44

Indeed, in BaLi₂In₂Ge₂, there is a sizable orbital contribution from all atomic sites at the Fermi level. The considerable

hybridization persists even well below $E_{\rm F}$ down to about $E-E_{\rm F}=-7.5$ eV. Below this energy, localized states displaying primarily Ge(4s) character are situated. They correspond to the lone pairs of the Ge atoms in the structure. A comparable electronic spectrum was determined for the structurally similar BaMg₂Li₂Ge₂ (Figure S3 in the Supporting Information). It is worthwhile to note that, despite the substantial mixing of the electronic states, the formal charge assignment (Ba²⁺)-(Li⁺)₂(In²⁺)₂(Ge⁴⁻)₂ appears to be a reasonable approximation, as suggested by the calculated Bader charges: Ba, +1.57; Li, +0.98; In, +1.73; Ge, -3.49.

Analysis of the chemical bonding using crystal orbital Hamilton population curves (COHP) shows that, for the Ba—Ge and Ba—In contacts, the interactions are of purely bonding nature and are somewhat underoptimized at $E_{\rm F}$, with the negative integrated COHP values at the Fermi level (–ICOHP) of 0.41 eV/bond and 0.06 eV/bond for the Ba—Ge and Ba—In contacts, respectively (Figure 4b).

Other interactions in the structure appear to be more complex. They display combinations of states having different characters below the Fermi level. For the two symmetrically independent Li–Ge contacts, the competition between the bonding and antibonding interactions results in almost optimized bonding at $E_{\rm F}$, with strikingly different –ICOHP magnitudes of 0.56 and 0.06 eV/bond for the shorter and longer contacts, respectively (Figure 4c). Interestingly, the two Li–In contacts, which also demonstrate notably different lengths, are found to have a much smaller spread of the –ICOHP values, with 0.24 and 0.18 eV/bond, with the first value corresponding to the shorter Li–In bond (Figure 4d). The small difference in the –ICOHP numbers likely indicates a more delocalized nature of the Li–In interactions in comparison with Li–Ge.

Whereas the In–Ge contact shows almost exclusively bonding character below $E_{\rm F}$, the In–In interaction is hallmarked by the presence of bonding and antibonding peaks in the COHP curve (Figure 4e). Both bonds are optimized at the Fermi level and display similar –ICOHP magnitudes of 1.64 and 1.58 eV/bond for In–Ge and In–In, respectively. Such large values point toward strong covalent bonding. In accordance with the COHP analysis, examination of the electron localization function (ELF) distribution reveals a localized domain in the middle of the In–In contact, corresponding to a nonpolar covalent interaction, and flattening of the ELF around the Ge atoms, perpendicular to the In–Ge contacts, indicating polar covalent bonding (Figure 4f).

Electrical Transport Properties. The temperature dependence of the electrical resistivity for a SrLi₂In₂Ge₂ single crystal is shown in Figure 5. In accordance with our first-

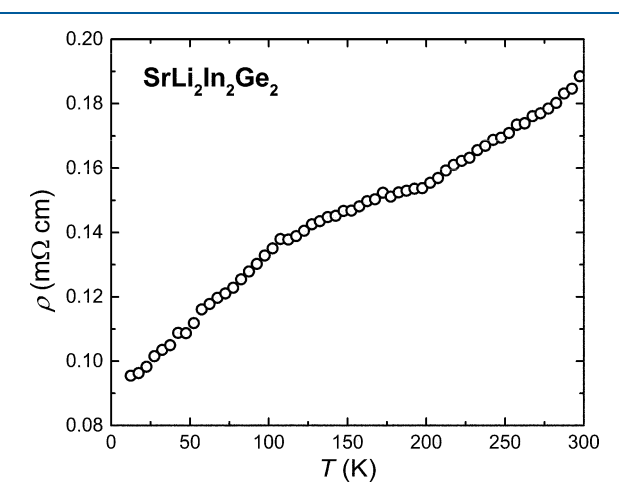


Figure 5. Temperature dependence of electrical resistivity measured on a single crystal of SrLi₂In₂Ge₂.

principles calculations, the studied compound displays metallic behavior in the whole measured temperature range. However, the $\rho(T)$ curve does not follow a simple linear dependence at high temperatures, which would be expected for typical metals. This might be related to short mean free paths of charge carriers resulting from extensive scattering. The room-temperature resistivity is on the order of 10^{-1} m Ω cm, which is comparable to the values found in some Ge-based clathrates, e.g., the type-I $\mathrm{Sr_8Zn_8Ge_{38}}^{.45}$ Altogether, $\mathrm{SrLi_2In_2Ge_2}$ exhibits properties typical for bad metals. Similar behavior was previously reported for other formally electron-precise

germanides, such as $Ca_5Ge_3^{\ 43}$ and $CaGe_2^{\ 47}$ both showing pseudogaps at the Fermi level in their electronic structures.

CONCLUSIONS

The quaternary compounds $AELi_2In_2Ge_2$ (AE = Sr, Ba, Eu) constitute a new structural family of formally electron-precise germanides. The crystal structure of these phases is described as an ordered quaternary derivative of the CaCu₄P₂ structure type. The charge balance in $AELi_2In_2Ge_2$ (AE = Sr, Ba, Eu) is achieved owing to the formation of homoatomic In-In bonds. The interactions between the In atoms in the two-dimensional [In₂Ge₂] slabs can be disrupted by the partial substitution of Li for In atoms, as shown for the BaLi_{2+x}In_{2-x}Ge₂ solid solution. Li/In mixing up to the ratio 2:1 allows the average structure to be retained, although the chemical bonding is subtly different. On the basis of the structural analysis and consideration of the valence electron count, it can be suggested that the limiting member of the BaLi_{2+x}In_{2-x}Ge₂ solid solution on the "Li-rich" side is the phase where one-third of the In atoms are replaced by Li atoms ($x \approx 0.66$), whereas the phase BaLi₂In₂Ge₂, in which there is no disorder, is the end member on the "Li-poor" side. First-principles calculations and electrical transport measurements indicate metallic behavior of the studied compounds. Considerable hybridization of the electronic states prevents opening of a band gap, resulting in the Fermi level located inside a pseudogap instead. The low values of the electrical resistivity and the apparent electronic stability of the average crystal structure against small variations makes the title compounds interesting candidates for electrochemical testing, providing that further optimization of the synthetic conditions yields single-phase samples in bulk quantities.

ASSOCIATED CONTENT

S Supporting Information

The Supporting Information is available free of charge on the ACS Publications website at DOI: 10.1021/acs.inorg-chem.9b00588.

Crystal structure representation, atomic coordinates, and selected interatomic distances of BaLi_{1.02(2)}In_{0.98}Ge₂ and electronic densities of states for SrLi₂In₂Ge₂ and BaMg,Li₂Ge₂ (PDF)

Accession Codes

CCDC 1899716–1899721 contain the supplementary crystallographic data for this paper. These data can be obtained free of charge via www.ccdc.cam.ac.uk/data_request/cif, or by emailing data_request@ccdc.cam.ac.uk, or by contacting The Cambridge Crystallographic Data Centre, 12 Union Road, Cambridge CB2 1EZ, UK; fax: +44 1223 336033.

AUTHOR INFORMATION

Corresponding Author

*S.B.: e-mail, bobev@udel.edu; tel, (302)-831-8720; fax, (302)-831-6335.

ORCID

Svilen Bobev: 0000-0002-0780-4787

Author Contributions

The manuscript was written through contributions of all authors. All authors have given approval to the final version of the manuscript.

Notes

The authors declare no competing financial interest.

ACKNOWLEDGMENTS

This work was supported by the National Science Foundation under Award # NSF DMR-1709813. The authors are indebted to Dr. T.-S. You for conducting the early exploratory studies in the Sr-Li-In-Ge and Ba-Li-In-Ge systems. We also acknowledge the anonymous reviewer who gave very interesting suggestions pertaining to the structure rationalization and the understanding of the chemical bonding.

REFERENCES

- (1) Tarascon, J.-M.; Armand, M. Issues and Challenges Facing Rechargeable Lithium Batteries. *Nature* **2001**, 414 (6861), 359–367.
- (2) Goodenough, J. B.; Kim, Y. Challenges for Rechargeable Li Batteries. *Chem. Mater.* **2010**, 22 (3), 587–603.
- (3) Goriparti, S.; Miele, E.; De Angelis, F.; Di Fabrizio, E.; Proietti Zaccaria, R.; Capiglia, C. Review on Recent Progress of Nanostructured Anode Materials for Li-Ion Batteries. *J. Power Sources* **2014**, 257, 421–443.
- (4) Anasori, B.; Lukatskaya, M. R.; Gogotsi, Y. 2D Metal Carbides and Nitrides (MXenes) for Energy Storage. *Nat. Rev. Mater.* **2017**, 2 (2), 16098.
- (5) Li, Y.; Raghavan, R.; Wagner, N. A.; Davidowski, S. K.; Baggetto, L.; Zhao, R.; Cheng, Q.; Yarger, J. L.; Veith, G. M.; Ellis-Terrell, C.; Miller, M. A.; Chan, K. S.; Chan, C. K. Type I Clathrates as Novel Silicon Anodes: An Electrochemical and Structural Investigation. *Adv. Sci.* **2015**, *2* (6), 1500057.
- (6) Ovchinnikov, A.; Bobev, S. Zintl Phases with Group 15 Elements and the Transition Metals: A Brief Overview of Pnictides with Diverse and Complex Structures. *J. Solid State Chem.* **2019**, 270, 346–359.
- (7) Zhao, R.; Bobev, S.; Krishna, L.; Yang, T.; Weller, J. M.; Jing, H.; Chan, C. K. Anodes for Lithium-Ion Batteries Based on Type I Silicon Clathrate Ba₈Al₁₆Si₃₀ Role of Processing on Surface Properties and Electrochemical Behavior. *ACS Appl. Mater. Interfaces* **2017**, 9 (47), 41246–41257.
- (8) Dopilka, A.; Zhao, R.; Weller, J. M.; Bobev, S.; Peng, X.; Chan, C. K. Experimental and Computational Study of the Lithiation of Ba₈Al_yGe_{46-y} Based Type I Germanium Clathrates. *ACS Appl. Mater. Interfaces* **2018**, *10* (44), 37981–37993.
- (9) You, T.-S.; Bobev, S. Cis-Trans Germanium Chains in the Intermetallic Compounds $ALi_{1-x}In_xGe_2$ and $A_2(Li_{1-x}In_x)_2Ge_3$ (A = Sr, Ba, Eu)—Experimental and Theoretical Studies. *J. Solid State Chem.* **2010**, 183 (12), 2895–2902.
- (10) Nam, G.; Jang, E.; You, T.-S. Site-Preference among Three Anions in the Quaternary BaAl₄-Type Structure: Experimental and Computational Investigations for BaLi_{1.09(1)}In_{0.91}Ge₂. Bull. Korean Chem. Soc. **2013**, 34 (12), 3847–3850.
- (11) Zintl, E.; Brauer, G. Über die Valenzelektronenregel und die Atomradien unedler Metalle in Legierungen. (10. Mitteilung über Metalle und Legierungen). Z. Phys. Chem. B 1933, 20B, 245–271.
- (12) Zürcher, F.; Wengert, S.; Nesper, R. Crystal Structure of Barium Dimagnesium Dilithium Disilicide, BaMg₂Li₂Si₂, and of Barium Dimagnesium Dilithium Digermanide, BaLi₂Mg₂Ge₂. Z. Kristallogr.-New Cryst. Struct. **2001**, 216 (4), 503–504.
- (13) Vaughey, J. T.; Miller, G. J.; Gravelle, S.; Alejandro Leon-Escamilla, E.; Corbett, J. D. Synthesis, Structure, and Properties of BaGe₂: A Study of Tetrahedral Cluster Packing and Other Three-Connected Nets in Zintl Phases. *J. Solid State Chem.* **1997**, *133* (2), 501–507.
- (14) Bentien, A.; Nishibori, E.; Paschen, S.; Iversen, B. B. Crystal Structures, Atomic Vibration, and Disorder of the Type-I Thermoelectric Clathrates Ba₈Ga₁₆Si₃₀, Ba₈Ga₁₆Ge₃₀, Ba₈In₁₆Ge₃₀, and Sr₈Ga₁₆Ge₃₀. *Phys. Rev. B: Condens. Matter Mater. Phys.* **2005**, 71 (14), 144107.
- (15) Mao, J.-G.; Xu, Z.; Guloy, A. M. Synthesis and Crystal Structure of Ae_2 LiInGe₂ (Ae = Ca, Sr): New Zintl Phases with a Layered Silicate-like Network. *Inorg. Chem.* **2001**, 40 (17), 4472–4477.

(16) You, T.-S.; Bobev, S. Diytterbium(II) Lithium Indium(III) Digermanide, Yb₂LiInGe₂. *Acta Crystallogr., Sect. E: Struct. Rep. Online* **2010**, *66* (5), i43—i43.

- (17) SAINT: Bruker AXS: Madison, WI, USA, 2014.
- (18) SADABS; Bruker AXS: Madison, WI, USA, 2014.
- (19) Sheldrick, G. M. SHELXT Integrated Space-Group and Crystal-Structure Determination. Acta Crystallogr., Sect. A: Found. Adv. 2015, 71 (1), 3–8.
- (20) Sheldrick, G. M. Crystal Structure Refinement with SHELXL. Acta Crystallogr., Sect. C: Struct. Chem. 2015, 71 (1), 3–8.
- (21) Gelato, L. M.; Parthé, E. STRUCTURE TIDY a Computer Program to Standardize Crystal Structure Data. J. Appl. Crystallogr. 1987, 20 (2), 139–143.
- (22) Jepsen, O.; Andersen, O. K. *The Stuttgart TB-LMTO-ASA Program, Version 4.7*; Max-Planck-Institut für Festkörperforschung: Stuttgart, Germany.
- (23) von Barth, U.; Hedin, L. A Local Exchange-Correlation Potential for the Spin Polarized Case: I. J. Phys. C Solid State Phys. 1972, 5 (13), 1629–1642.
- (24) Otero-de-la-Roza, A.; Johnson, E. R.; Luaña, V. Critic2: A Program for Real-Space Analysis of Quantum Chemical Interactions in Solids. *Comput. Phys. Commun.* **2014**, *185* (3), 1007–1018.
- (25) Mewis, A. Darstellung und Struktur der Verbindung CaCu₄P₂. Z. Naturforsch., B. J. Chem. Sci. 1980, 35 (8), 942–945.
- (26) He, H.; Stearrett, R.; Nowak, E. R.; Bobev, S. Gallium Pnictides of the Alkaline Earth Metals, Synthesized by Means of the Flux Method: Crystal Structures and Properties of $CaGa_2Pn_2$, $SrGa_2As_2$, $Ba_2Ga_3As_5$, and $Ba_4Ga_5Pn_8$ (Pn = P or As). Eur. J. Inorg. Chem. **2011**, 2011 (26), 4025–4036.
- (27) Pardo, M. P.; Flahaut, J. Sur une nouvelle forme de GaS, rhomboedrique 3R metastable formation et etude structurale. *Mater. Res. Bull.* 1987, 22 (3), 323–329.
- (28) Fedorchuk, A.; Prots, Y.; Grin, Y. Crystal Structures of Europium Magnesium Gallium, Eu Mg_xGa_{4-x} , and Europium Lithium Gallium, Eu Li_xGa_{4-x} (x=0.5). Z. Kristallogr.-New Cryst. Struct. **2005**, 220 (3), 317–318.
- (29) Ojwang, D. O.; Bobev, S. Synthesis and Structural Characterization of $Ba_7Li_{11}Bi_{10}$ and $AE_4(Li,Tr)_7Pn_6$ (AE = Sr, Ba, Eu; Tr = Ga, In; Pn = Sb, Bi). Inorganics **2018**, 6 (4), 109.
- (30) Makongo, J. P. A.; Bobev, S. The Series $RE_5 \text{Li}_2 \text{Sn}_7$ (RE = Ce, Pr, Nd, Sm) Revisited: Crystal Structure of $RE_5 \text{Li}_{2-x} \text{Sn}_{7+x}$ [$0 \le x \le 0.03(1)$]. Acta Crystallogr., Sect. C: Struct. Chem. **2014**, 70 (1), 2–6.
- (31) Nesper, R. The Zintl-Klemm Concept A Historical Survey. Z. Anorg. Allg. Chem. 2014, 640 (14), 2639–2648.
- (32) Bobev, S.; Bauer, E. D.; Thompson, J. D.; Sarrao, J. L.; Miller, G. J.; Eck, B.; Dronskowski, R. Metallic Behavior of the Zintl Phase EuGe₂: Combined Structural Studies, Property Measurements, and Electronic Structure Calculations. *J. Solid State Chem.* **2004**, *177* (10), 3545–3552.
- (33) Gon Park, D.; Dong, Y.; DiSalvo, F. J. LiSrGe₂ and LiBaGe₂: One-Dimensional Chains of in an Unusual Conformation. *J. Alloys Compd.* **2009**, 470 (1–2), 90–95.
- (34) Bobev, S.; You, T.-S.; Suen, N.-T.; Saha, S.; Greene, R.; Paglione, J. Synthesis, Structure, Chemical Bonding, and Magnetism of the Series *RELiGe*₂ (*RE* = La–Nd, Sm, Eu). *Inorg. Chem.* **2012**, *S1* (1), 620–628.
- (35) Schäfer, M. C.; Yamasaki, Y.; Fritsch, V.; Bobev, S. Synthesis and Structural Characterization of ACu_9Tt_4 (A = Ca, Sr, Ba, Eu; Tt = Si, Ge, Sn) Tetragonally Distorted Ternary Variants of the Cubic NaZn₁₃ Structure Type. Improved Structure Refinement of SrCu₂Ge₂. *Z. Anorg. Allg. Chem.* **2012**, *638* (7–8), 1204–1211.
- (36) Seo, D.-K.; Corbett, J. D. Synthesis, Structure, and Bonding of Hypoelectronic SrIn₄: Direct Example of a Dominant Size Effect in Structure Selection. *J. Am. Chem. Soc.* **2000**, *122* (40), 9621–9627.
- (37) Amerioun, S.; Häussermann, U. Structure and Bonding of Sr₃In₁₁: How Size and Electronic Effects Determine Structural Stability of Polar Intermetallic Compounds. *Inorg. Chem.* **2003**, *42* (24), 7782–7788.

(38) Wendorff, M.; Röhr, C. Binäre Indide AIn_x (x=1,2,4;A=Ca, Sr, Ba, K, Rb) - Untersuchungen zu Strukturchemie und chemischer Bindung. Z. Anorg. Allg. Chem. **2005**, 631 (2–3), 338–349.

- (39) Pauling, L. The Nature of the Chemical Bond; Cornell University Press: Ithaca, NY, 1960.
- (40) Guo, S.-P.; You, T.-S.; Bobev, S. Closely Related Rare-Earth Metal Germanides $RE_2\text{Li}_2\text{Ge}_3$ and $RE_3\text{Li}_4\text{Ge}_4$ (RE = La-Nd, Sm): Synthesis, Crystal Chemistry, and Magnetic Properties. *Inorg. Chem.* **2012**, *51* (5), 3119–3129.
- (41) Suen, N.-T.; You, T.-S.; Bobev, S. Synthesis, Crystal Structures and Chemical Bonding of $RE_{5-x}Li_xGe_4$ (RE = Nd, Sm and Gd; $x \simeq 1$) with the Orthorhombic Gd_5Si_4 Type. Acta Crystallogr., Sect. C: Cryst. Struct. Commun. **2013**, 69 (1), 1–4.
- (42) Saparov, B.; He, H.; Zhang, X.; Greene, R.; Bobev, S. Synthesis, Crystallographic and Theoretical Studies of the New Zintl Phases $Ba_2Cd_2Pn_3$ (Pn=As, Sb), and the Solid Solutions ($Ba_{1-x}Sr_x$) $_2Cd_2Sb_3$ and $Ba_2Cd_2(Sb_{1-x}As_x)_3$. Dalton Trans. **2010**, 39 (4), 1063–1070.
- (43) Mudring, A.-V.; Corbett, J. D. Unusual Electronic and Bonding Properties of the Zintl Phase Ca₅Ge₃ and Related Compounds. A Theoretical Analysis. *J. Am. Chem. Soc.* **2004**, *126* (16), 5277–5281. (44) Aydemir, U.; Ormeci, A.; Borrmann, H.; Böhme, B.; Zürcher, F.; Uslu, B.; Goebel, T.; Schnelle, W.; Simon, P.; Carrillo-Cabrera, W.; Haarmann, F.; Baitinger, M.; Nesper, R.; von Schnering, H.-G.; Grin, Y. The Metallic Zintl Phase Ba₃Si₄ Synthesis, Crystal Structure, Chemical Bonding, and Physical Properties. *Z. Anorg. Allg. Chem.* **2008**, *634* (10), 1651–1661.
- (45) Qiu, L.; Swainson, I. P.; Nolas, G. S.; White, M. A. Structure, Thermal, and Transport Properties of the Clathrates $Sr_8Zn_8Ge_{38}$, $Sr_8Ga_{16}Ge_{30}$, and $Ba_8Ga_{16}Si_{30}$. Phys. Rev. B: Condens. Matter Mater. Phys. **2004**, 70 (3), No. 035208.
- (46) Ovchinnikov, A.; Bobev, S. Synthesis, Crystal and Electronic Structure of the Titanium Bismuthides $Sr_5Ti_{12}Bi_{19+x}$, $Ba_5Ti_{12}Bi_{19+x}$, and $Sr_5_{-\delta}Eu_{\delta}Ti_{12}Bi_{19+x}$ ($x \approx 0.5-1.0$; $\delta \approx 2.4$, 4.0). Eur. J. Inorg. Chem. **2018**, 2018 (11), 1266–1274.
- (47) Tobash, P. H.; Bobev, S. Synthesis, Structure and Electronic Structure of a New Polymorph of CaGe₂. *J. Solid State Chem.* **2007**, 180 (5), 1575–1581.